Polymer electrolyte membrane fuel cell grade hydrogen production by methanol steam reforming: A comparative multiple reactor modeling study

CrossMark

Nisha Katiyar, Shashi Kumar, Surendra Kumar*

Department of Chemical Engineering, Indian Institute of Technology Roorkee, Roorkee, Uttarakhand 247667, India

HIGHLIGHTS

- A noble process scheme to generate pure H_2 is proposed.
- High residence time enhances H_2 recovery and H_2 yield.
- Exit gas composition is reduced to permissible discharge limit.
- Produced pure H_2 can operate a 470 W PEMFC stack.

ARTICLE INFO

ABSTRACT

Analysis of a fuel processor based on methanol steam reforming has been carried out to produce fuel cell grade H_2. Six reactor configurations namely FBR1 (fixed bed reactor), MR1 (H_2 selective membrane reactor with one reaction tube), MR2 (H_2 selective membrane reactor with two reaction tubes), FBR2 (FBR1 + preferential CO oxidation (PROX) reactor), MR3 (MR1 + PROX), and MR4 (MR2 + PROX) are evaluated by simulation to identify the suitable processing scheme. The yield of H_2 is significantly affected by H_2 selective membrane, residence time, temperature, and pressure conditions at complete methanol conversion. The enhancement in residence time in MR2 by using two identical reaction tubes provides H_2 yield of 2.96 with 91.25 mol% recovery at steam/methanol ratio of 1.5, pressure of 2 bar and 560 K temperature. The exit retentate gases from MR2 are further treated in PROX reactor of MR4 to reduce CO concentration to 4.1 ppm to ensure the safe discharge to the environment. The risk of carbon deposition on reforming catalyst is highly reduced in MR4, and MR4 reactor configuration generates 7.4 NL min^{-1} of CO free H_2 from 0.12 mol min^{-1} of methanol which can provide 470 W PEMFC feedstock requirement. Hence, process scheme in MR4 provides a compact and innovative fuel cell grade H_2 generating unit.

1. Introduction

In last few decades, fuel cells have attracted considerable attention as leading power generating engines due to their high efficiency and low emission of pollutants. Among many types of fuel cells, polymer electrolyte membrane (PEM) fuel cell used widely in mobile and stationary applications, has received increased attention due to their attractive features such as high energy density, rapid start up and response, low operating temperatures and compactness [1]. Hydrogen is used as a fuel for PEM fuel cell. For portable fuel cells applications, a fuel processor using high energy renewable liquid fuels to produce on board H_2 is desirable [2–4]. Methanol, a renewable liquid fuel, is recognized as a promising and potential fuel for hydrogen production. Methanol offers a number of advantages for H_2 production via catalytic reforming as it can be reformed at low temperatures (473–573 K) and provides high H/C ratio compared to other hydrocarbons [5,6]. Hydrogen is obtained from methanol using various catalytic reforming processes such as steam reforming, decomposition, oxidative steam reforming, partial oxidation and autothermal reforming. Among these processes, steam reforming is the most widely used industrial process for large scale production of hydrogen [7,8].

Methanol steam reforming is carried out over various non-noble metal (Cu, Ni) catalysts and noble metal catalysts (Pd, Pt, Rh) [9–13]. During reforming, formation of many undesired products

* Corresponding author. Tel.: +91 9897077460; fax: +91 1332 273560.
  E-mail address: skumar.iitroorkee@gmail.com (S. Kumar).

reduces the quantity and quality of desired product H_2. It is well known that PEM fuel cell requires highly pure H_2 containing CO less than 10 ppm. High CO content ($\geq$10 ppm) leads to detrimental effect on low temperature PEM fuel cell performance [14]. For this reason, many research works have been reported in the literature to treat reformate gas before sending to fuel cell. In these studies, the reformer has been followed by the combinations of low temperature water gas shift (WGS) reactor, high temperature WGS reactor, preferential CO oxidation (PROX) reactor, and pressure swing adsorption unit [2,15,16]. Thus, the whole fuel processing unit becomes quite difficult to carry and handle, and cannot be comfortably used in automotive fuel cell applications [17]. Additionally as a general outcome, these combinations provide low content of H_2 with large amount of CO_2 which on feeding fuel cell stack, reduces the fuel cell efficiency. Therefore, a recent research debate is emerging over fuel cell grade H_2 production in a compact device. The reformer equipped with H_2 selective membrane provides a compact device to get pure hydrogen stream from the outlet of the reformer. This H_2 stream can be directly sent to PEM fuel cell. In the literature, very few studies are reported which are concerned with the methanol reforming in the membrane reactor [18,19].

The catalytic reformer equipped with H_2 selective membrane increases the methanol conversion by shifting the equilibrium of reforming reaction toward product formation, and thus enhances the production of H_2 [20]. It is known that Pd and Pd-alloy dense membranes are highly hydrogen selective membranes and exhibit good mechanical stability. Alloying Pd with Ag membrane offers high permeation rate of H_2, good stability as well as lower material cost [21]. Removal of H_2 from the reformate gas through H_2 selective membrane increases the conversion of CO via water gas shift reaction to produce more H_2 and thereby reduces the CO concentration. The concentration of CO, however, is far away from the permissible limit. Therefore, preferential CO oxidation (PROX) reactor may be hooked up with the reformer to reduce CO.

In the present modeling work, one dimensional steady state mathematical models have been developed for fixed bed reactor and fixed bed membrane reactor. Three types of reactors namely, fixed catalytic bed reforming reactor, fixed catalytic bed H_2 selective membrane reactor for reforming, and fixed catalytic bed reactor for preferential oxidation of CO are considered. Six reactor configuration modules are selected for simulation where each reactor configuration consists of either one reactor or two reactors with identical dimensions connected in series. The simulations are carried out to

compare the performance of each reactor configuration. Two schemes are explored to identify the possibility of getting either fuel cell grade H_2 with high yield or pure H_2 with high yield in conjunction with emission of exit gases within permissible discharge limits. New corrected H_2 permeation rate through H_2 selective Pd-alloy membrane is incorporated in the model by considering all inhibiting effects of coexisting gaseous components. Additionally, the reactor configuration in which minimum carbon formation occurs on the catalyst has been identified thermodynamically.

2. Kinetic model

Various possible reaction routes have been proposed for converting methanol into hydrogen through many intermediate formation reactions. Katiyar et al. [8] carried out thermodynamic analysis on methanol steam reforming and reviewed the literature to assess the possibility of formation of various intermediates and undesired products such as CH_4, which might depend on the use of various types of catalyst. Highly undesired methanation and carbon formation reactions are found thermodynamically feasible. They identified that the Cu-based catalysts were the most efficient and suitable catalysts for the production of fuel cell grade hydrogen by methanol steam reforming. In view of these findings, most widely accepted route for hydrogen production by methanol steam reforming contains three reactions namely, steam reforming of methanol (SRM), methanol decomposition (MD), and water gas shift (WGS), represented as R_1–R_3 respectively (Table 1). Since undesired methanation reactions responsible for CH_4 production are completely kinetically suppressed on Cu-based catalyst [8], these reactions are not considered in the present study.

Although, many kinetic models for methanol steam reforming on Cu-based catalysts are available in the literature [22–28], the most reliable and widely used intrinsic kinetic model given by Peppley et al. [22] on $Cu/ZnO/Al_2O_3$ catalyst is considered in the present work. Peppley et al. [22] carried out steam reforming of methanol in a conventional isothermal fixed bed tubular reactor in the presence of $Cu/ZnO/Al_2O_3$ catalyst with composition as 40/40/20 (wt%). The reactor consisted of 0.30 m long stainless steel pipe with 0.0221 m inner diameter. In order to explain the complete range of observed product compositions in kinetic analysis, three reactions namely steam reforming of methanol, methanol decomposition and water gas shift reactions were included in the kinetic analysis. Although, the methanol decomposition was observed to

Table 1
Reactions and reaction rate expressions for reformer and PROX reactor.

Reactions		Rate expressions	Eq. no.
Reformer ($Cu/ZnO/Al_2O_3$ Catalyst) [22]			
(R_1)	SRM	$r_1 = \dfrac{k_1 K_1 (p_{tCH_3OH} - (p_{tH_2}^3 p_{tCO_2}/K_{R_1,T} p_{tH_2O})) C_{S1} C_{S1a} S_g}{(p_{tH_2}^{0.5} + K_1 p_{tCH_3OH} + K_2 p_{tCO_2} p_{tH_2} + K_3 p_{tH_2O})(1 + K_4^{0.5} p_{tH_2}^{0.5})}$	(1)
	$CH_3OH + H_2O \leftrightarrow CO_2 + 3H_2$		
	$\Delta H_{jT_0} = +49.24$		
(R_2)	MD	$r_2 = \dfrac{k_2 K_5 (p_{tCH_3OH} - (p_{tH_2}^2 p_{tCO}/K_{R_2,T})) C_{S2} C_{S2a} S_g}{(p_{tH_2}^{0.5} + K_5 p_{tCH_3OH} + K_6 p_{tH_2O})(1 + K_7^{0.5} p_{tH_2}^{0.5})}$	(2)
	$CH_3OH \leftrightarrow CO + 2H_2$		
	$\Delta H_{jT_0} = +90.41$		
(R_3)	WGS	$r_3 = \dfrac{k_3 K_1 p_{tH_2}^{0.5} (p_{tCO} p_{tH_2O} - (p_{tH_2} p_{tCO_2}/K_{R_3,T})) C_{S1}^2 S_g}{(p_{tH_2}^{0.5} + K_1 p_{tCH_3OH} + K_2 p_{tCO_2} p_{tH_2} + K_3 p_{tH_2O})^2}$	(3)
	$CO + H_2O \leftrightarrow CO_2 + H_2$		
	$\Delta H_{jT_0} = -41.17$		
PROX Reactor (Pt–Fe–Al_2O_3 Catalyst) [2]			
(R_4)	CO Oxidation	$r_4 = 3.528 \times 10^2 e^{(-33,092/RT)} p_{tO_2}^{0.5} p_{tCO}^{-0.1}$	(4)
	$CO + 0.5O_2 \leftrightarrow CO_2$		
	$\Delta H_{jT_0} = -283$		
(R_5)	H_2 Oxidation	$r_5 = 20.53 e^{(-18,742/RT)} p_{tO_2}^{0.5}$	(5)
	$H_2 + 0.5O_2 \leftrightarrow H_2O$		
	$\Delta H_{jT_0} = -241.81$		
(R_6)	WGS	$r_6 = 4.402 \times 10^3 e^{(-34,104/RT)} \left(p_{tCO} p_{tH_2O} - \dfrac{p_{tCO_2} p_{tH_2}}{K_{R_3,T}} \right)$	(6)
	$CO + H_2O \leftrightarrow CO_2 + H_2$		
	$\Delta H_{jT_0} = -41.17$		

occur on a different types of active site and was much slower than steam reforming of methanol and water gas shift reactions, methanol decomposition was included in the kinetic study because very small amount of CO adversely affected the performance of low temperature fuel cell. The configuration of the packed bed was designed to ensure that temperature gradients and axial dispersion were negligible, and there were no significant internal mass transfer gradients. The effects of pressure (1–33 bar), temperature (433–533 K), and feed composition ($S/M = 1$) on catalyst activity, selectivity and rate of deactivation were estimated for kinetic analysis. In the kinetic model, Langmuir–Hinshelwood expressions were derived by kinetic analysis of elementary surface reactions occurring on the catalyst for three reversible reactions. The variation in the CO content and rate of hydrogen production were analyzed. Dual site surface mechanisms were considered on the catalyst surface. Type-1 active site promoted the methanol steam reforming and water gas shift reactions while methanol decomposition reaction was highly active on the Type-2 active site. In addition, the rate determining step (RDS) was the dehydrogenation of adsorbed methoxy groups for both SMR and MD reactions whereas for WGS, the RDS was the formation of an intermediate formate species. All required parameters for kinetic model were estimated by a multi-response non-linear regression. The resultant comprehensive kinetic model is able to analyze the rates of production of H_2, CO_2 and CO over the wide range of operating conditions including high pressure (33 bar). The kinetic expressions for reactions R_1–R_3 as well as the kinetic parameters employed for the calculation of the reaction rates, are summarized in Tables 1 and 2. The temperature dependent expressions for equilibrium constants $K_{j,T}$ are taken from the studies of Katiyar et al. [8].

In order to prevent poisoning of the fuel cell electrodes by CO, the reformer is followed by CO-cleanup equipment. Amongst few methods, the catalytic oxidation of CO is considered as one of the most successfully adopted and economically viable methods. The oxidation of CO is accompanied by water gas shift reaction and undesired oxidation of H_2. It is carried out in preferential CO oxidation (PROX) reactor where the air stream is co-fed with the reformate exit gas at the inlet of the PROX reactor. All involved reactions are represented in Table 1 by R_4–R_6. These reactions are studied on a commercial Pt–Fe–Al_2O_3 catalyst by Choi and Stenger [2]. In the reaction test units, Choi and Stenger [2] considered three reactions namely CO oxidation, H_2 oxidation and water gas shift. They performed these reactions in a stainless steel tubular reactor with 0.0127 m inner diameter and 0.30 m length in the presence of Pt–Fe–Al_2O_3 catalyst. The used catalyst was 3 mm × 4 mm sized pellets composed of 0.5% Pt and 0.02% Fe on a γ-Al_2O_3 support. The catalyst pellets were ground to reduce the particle size in the range of 100–250 μm to ensure that internal diffusional resistances were negligible and good gas distribution was allowed. The reaction conditions such as feed flow rate and pressure were chosen similar to the fuel processor system. All reaction tests were performed at temperatures between 393 and 598 K, at 1 bar pressure and O_2/CO molar ratio between 1 and 2. They derived the empirical rate

expressions for three reversible reactions by using power law kinetic model. These rate expressions are given in Table 1.

The net rate of formation of component i (r_i) is represented by

$$r_i = \sum_{j=1}^{M} \eta_j (\pm \nu_{ij} r_j) \tag{7}$$

In Eq. (7), η_j is the effectiveness factor for jth reaction and ν_{ij} is the stoichiometric coefficient of ith component in jth reaction. '+' sign with ν_{ij} indicates the formation of ith component in jth reaction whereas '−' sign is for the consumption of ith component in jth reaction. On the basis of Eq. (7), the net rates of formation of gaseous species in reformer and in PROX reactor can be written as follows:

Reformer

$$r_{CH_3OH} = -\eta_1 r_1 - \eta_2 r_2 \tag{7a}$$

$$r_{H_2O} = -\eta_1 r_1 - \eta_3 r_3 \tag{7b}$$

$$r_{H_2} = 3\eta_1 r_1 + 2\eta_2 r_2 + \eta_3 r_3 \tag{7c}$$

$$r_{CO} = \eta_2 r_2 - \eta_3 r_3 \tag{7d}$$

$$r_{CO_2} = \eta_1 r_1 + \eta_3 r_3 \tag{7e}$$

PROX Reactor

$$r_{CO}^* = -\eta_4 r_4 - \eta_6 r_6 \tag{7f}$$

$$r_{O_2}^* = -0.5\eta_4 r_4 - 0.5\eta_5 r_5 \tag{7g}$$

$$r_{H_2}^* = -\eta_5 r_5 + \eta_6 r_6 \tag{7h}$$

$$r_{CO_2}^* = \eta_4 r_4 + \eta_6 r_6 \tag{7i}$$

$$r_{H_2O}^* = \eta_5 r_5 - \eta_6 r_6 \tag{7j}$$

For a catalytic reaction, it is necessary to determine effectiveness factor for accurate prediction of its reaction rate which depends upon catalyst properties. Sufficiently small size of the catalyst particles, as in the case of packed bed reactors, results in negligibly small thermal and concentration gradients in the catalyst particle [30]. Due to this reason, the intraparticle mass transfer resistance and thereby effect of pore diffusion on reaction rates can be neglected for such situations. As a result, the actual reaction rate (i.e. rate with pore diffusion) becomes equal to the intrinsic reaction rate (i.e. rate without pore diffusion), leading to constant effectiveness factor of unity for all the reactions. Thus in the present study, the effectiveness factor of unity has been considered for all reactions. Thus, Eqs. (7a)–(7j) can be modified by putting $\eta_j = 1.0$. For large size catalyst particles (generally employed in industrial reactor), however, intraparticle mass transfer resistances must be taken into account, resulting in the effectiveness factor to be less than unity.

3. Permeation model

The membrane reactor couples the reaction and the separation in the same unit. Pd/Pd-alloy membranes are well known for their

Table 2
Kinetic constants and hydrogen permeation parameters [22,29].

$k_1 = 7.4 \times 10^{14} e^{(-12364.69/T)}$	$K_8 = 3.33 \times 10^{-10} e^{(58,462/RT)}$
$k_2 = 3.8 \times 10^{20} e^{(-20447.44/T)}$	$K_9 = 1.54 \times 10^{-10} e^{(49,114/RT)}$
$k_3 = 5.9 \times 10^{13} e^{(-10536.45/T)}$	$K_{10} = 6.38 \times 10^{-11} e^{(88,423/RT)}$
$K_1 = 6.55 \times 10^{-3} e^{(2405.58/T)}$	$K_{11} = 3.67 \times 10^{-15} e^{(106,217/RT)}$
$K_2 = 2.3 \times 10^{9} e^{(-12027.91/T)}$	$K_{12} = 1.69 \times 10^{-16} e^{(123,367/RT)}$
$K_3 = 4.74 \times 10^{-3} e^{(2405.58/T)}$	$K_{13} = 3.77 \times 10^{38} e^{(-418,858/RT)}$
$K_4 = 5.43 \times 10^{-6} e^{(6013.95/T)}$	$K_{14} = 4.44 \times 10^{29} e^{(-328,792/RT)}$
$K_5 = 36.9 e^{(2405.58/T)}$	C_{S1}, C_{S1a}: 7.5×10^{-6} mol m^{-2}
$K_6 = 36.9 e^{(2405.58/T)}$	C_{S2}, C_{S2a}: 1.5×10^{-5} mol m^{-2}
$K_7 = 3.86 \times 10^{-3} e^{(6013.95/T)}$	S_g: 1.02×10^{-5} m^2 kg^{-1}

ability to permeate H_2 with 100% permselectivity. H_2 permeation through Pd/Pd-alloy membrane follows the dissociation–solution diffusion transport mechanism and is governed by the difference in H_2 partial pressures at the interface of the high and low pressure sides of membrane reactor which acts as driving free. The hydrogen permeation flux through membrane can be written as follows:

$$J_{H_2} = \frac{P_{MH_2}}{\delta} \left[p_{tH_2}^n - p_{sH_2}^n \right] \tag{8}$$

where J_{H_2} is hydrogen flux, P_{MH_2} is the hydrogen permeation co-efficient, p_{tH_2} and p_{sH_2} are the partial pressures of H_2 in the high pressure (reaction or retentate side) and low pressure (permeate side) sides of the membrane respectively, and δ is the membrane thickness. The value of 'n' is used as an indicator for the rate controlling step of the permeation through Pd/Pd-alloy composite membrane [31]. When the Sievert's law is applied, the hydrogen flux becomes directly proportional to the difference of the square root of the hydrogen partial pressures on both sides of the membrane (i.e. $n = 0.5$). The permeability coefficient depends upon the temperature and can be described by Arrhenius Law in the following manner [32,33]:

$$P_{MH_2} = P_{MH_2,0} \times e^{-E_M/RT} \tag{9}$$

where $P_{MH_2,0}$, and E_M are the pre-exponential factor and the activation energy respectively. Gallucci and Basile [34] prepared the Pd/Ag thin wall membrane and conducted the experiments to estimate the parameters of Eqs. (8) and (9). Thus, the permeation flux of H_2 through Pd/Pd-alloy membrane is represented by Eq. (10)

$$J_{H_2} = \frac{P_{MH_2,0}}{\delta} \times e^{-29,160/RT} \left[p_{tH_2}^{0.5} - p_{sH_2}^{0.5} \right] \tag{10}$$

Several experimental studies have been carried out to investigate the effect of coexisting gaseous components on H_2 permeation through Pd/Pd-alloy membranes. Israni and Harold [20,29] conducted the experiments through 3.9 μm thick Pd/Ag alloy membrane at temperatures between 498 and 603 K. They found that the presence of H_2O, CO, and CO_2 inhibits the H_2 permeation and thus reduces the H_2 flux. The experimental observations indicated that the CO caused the largest drop in H_2 flux at temperature lower than 773 K. Unemoto et al. [35,36] conducted the experiments on 20 μm thick 23 wt% Pd/Ag alloy membrane. They concluded that at lower temperature, reduction of H_2 flux in the presence of H_2O, CO, and CO_2 was more. Whereas at temperature above 873 K, the inhibition effect on H_2 permeance was negligible. Gallucci et al. [37] worked on influence of H_2O, CO, CO_2, N_2 and Ar on the permeation flux through Pd/Ag alloy membrane. They found strong negative effect of CO on H_2 permeation in the temperature range 523–723 K and pressure 2–3.5 bar. Peters et al. [38], Mejdell et al. [39], Barbieri et al. [40], and Wilhite et al. [41] investigated the reduction in H_2 permeance due to presence of CO, CO_2 and H_2O at temperature between 548 and 623 K and reported strong negative effect of CO on H_2 permeance at lower temperatures. Steam reforming of methanol on Cu-based catalyst is carried out at temperature less than 623 K. Also, Pd/Ag alloy membranes possess high resistance to embrittlement below 623 K. The above study on H_2 flux through Pd/Ag membrane also reveals that the coexisting gaseous components specially CO have pronounced negative effect on H_2 flux at lower temperatures. Thus, it is necessary to modify the H_2 flux equation (Eq. (10)). Israni and Harold [29] and Barbieri et al. [40] quantified the reduction in H_2 flux through membrane in the presence of CH_3OH, H_2O, CO and CO_2 at different temperatures. They modified the H_2 permeation flux model through Pd-alloy membrane. They reported that primary reasons for the reduction included: reduced partial pressure of H_2 across the membrane, surface adsorption of the gaseous species other than H_2 and concentration polarization effects. On taking all these effects into account, following modified H_2 permeation flux expression was derived [29]:

$$J_{H_2} = \beta_C \frac{P_{MH_2,0}}{\delta} \times e^{-29,160/RT} \left[p_{tH_2}^{0.5} - p_{sH_2}^{0.5} \right] \tag{11}$$

$$\beta_C = \frac{\left(1 + \sqrt{K_8 p_{tH_2}}\right)}{1 + \sqrt{K_8 p_{tH_2}} + (K_9 p_{tH_2O}) + (K_{10} p_{tCO})^{1/3} + (K_{11} p_{tCO_2})^{1/2} + (K_{12} p_{tCH_3OH})^{1/2} + \frac{K_{13}\left(K_{12} p_{tCH_3OH}\right)}{\sqrt{K_8 p_{tH_2}}} + \frac{K_{13}K_{14}\left(K_{12} p_{tCH_3OH}\right)}{\left(K_8 p_{tH_2}\right)}} \tag{12}$$

Since the formation of CH_4 is not considered in the present work, the terms containing partial pressure of CH_4 in the model equation proposed by Israni and Harold [29] are set to zero to formulate Eq. (12). All the parameters used in Eq. (12) for membrane under study, are given in Table 2. The specifications of membrane and the values of permeation parameters are given in Table 3. The modified model Eq. (11) is suitable to evaluate the performance of membrane reactor for achieving pure H_2 for fuel cell application.

4. Modeling of reactors

The schematic diagrams of a fixed bed reactor (FBR) and membrane reactor (MR) under study are given in Fig. 1.

In FBR, the tube is packed with catalyst. The membrane reactor consists of two concentric tubes. The center tube is membrane tube and is packed with catalyst. This tube acts as a reaction zone. The outer shell tube represents permeation zone in which sweep gas is introduced to maintain the sufficient driving force for permeation by reducing the partial pressures of permeated gases. In the present study, composite dense Pd/Ag alloy membrane is used which consists of a dense Pd layer on the porous support. Since membrane is permeable only for hydrogen, no other gaseous component

Table 3
Operating parameters for simulation [42,43].

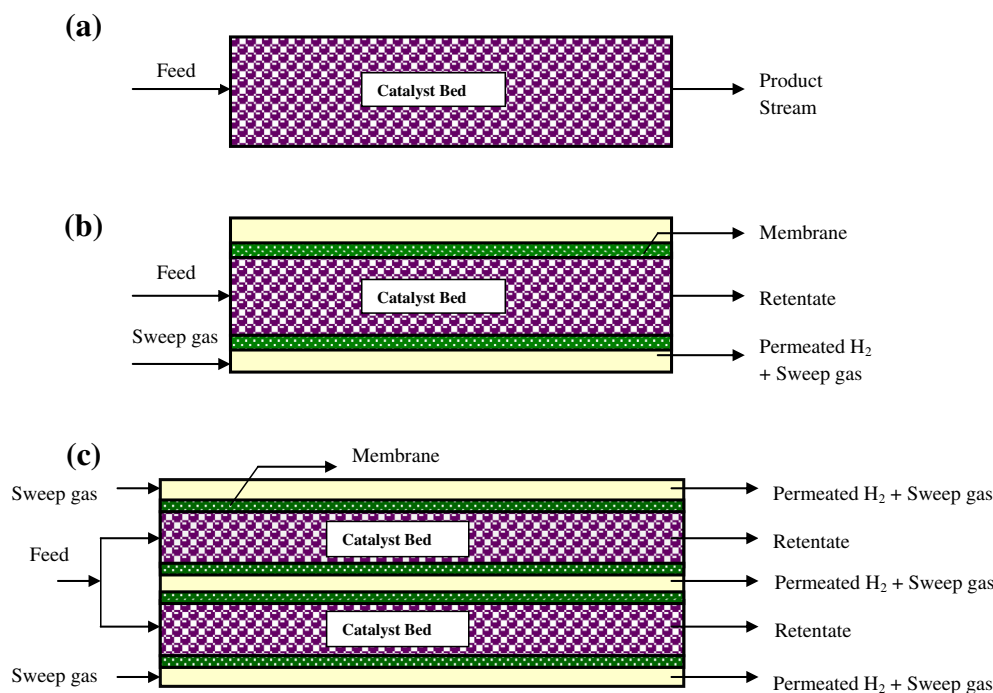|	
Reactor length L (m)	0.20
Inner diameter of reaction tube D_1 (m)	0.01
Particle diameter Dp (m)	6×10^{-4}
Pre-exponential factor $P_{MH_2,0}$ (mol m s^{-1} m^{-2} Pa$^{-0.5}$)	1.12×10^{-5}
Membrane thickness δ (m)	20×10^{-6}
R (J mol^{-1} K^{-1})	8.314
Inlet flow rate of methanol in feed $F_{tCH_3OH,0}$ (mol s^{-1})	2×10^{-3}
Steam to methanol feed ratio, S/M	1.5
Bed density of reformer ρ_B (kg m^{-3})	1300
Sweep ratio, SR	1–10

Fig. 1. Schematic representation of FBR1 (a), MR1 (b), and MR2 (c).

permeates through membrane from either side of the membrane. The sweep gas flows in co-current mode with respect to feed in the reaction zone.

In order to develop a one dimensional steady state mathematical model for FBR and MR reactors, following assumptions are taken: the transport mechanism is considered to be of plug flow type in the axial direction of both reaction and permeation zones of fixed bed and membrane reactors; since the ratio of the catalyst bed length ($L = 0.2$ m) to catalyst particle size (0.6×10^{-3} m) is greater than 50, both axial and radial dispersions can be neglected and, therefore, radial variation in temperature and concentration is not considered in the model [44–46]; the temperature and concentration gradients in the catalyst particle are neglected due to small particle size (far less than 3 mm) [44,45,47]; isobaric conditions are considered to prevail in the catalyst bed for gas phase reactions; the constant pressure on permeate side is assumed in membrane reactor as sweep gas flow rate is very high in comparison to the H_2 permeation rate; the reaction is carried out isothermally in the reactor. The isothermal condition can be justified by supplying sufficient heat from the wall of the fixed bed reactor to maintain the constant temperature. In the membrane reactor, the use of sweep gas in shell side can supply sufficient heat required to maintain the catalyst temperature in the reaction zone [46,48,49]; there is no mass and heat transfer resistances in the gas layer on both sides of the membrane; the membrane support does not offer mass transfer resistance to gas permeation due to macroporous structure. Therefore, the mass transfer resistance in the support layer is assumed to be negligible [50]; co-current flow of sweep gas is considered in the membrane reactor.

The mathematical model equations for fixed bed reactor and membrane reactor are represented by Eq. (13) and (14) respectively in Table 4. In order to analyze the performance of steam reforming of methanol for PEM fuel cell grade H_2 production, six reactor configurations abbreviated as FBR1, FBR2, MR1–MR4 are simulated (Figs. 1 and 2). The fixed bed reactor configuration FBR1 is conventional fixed bed reformer, and FBR2 is FBR1 followed by preferential CO oxidation (PROX) reactor. The PROX reactor is a fixed bed reactor packed with CO oxidation catalyst. The membrane reactor configuration MR1 represents membrane reactor with one packed reactor tube identical to FBR1 and tube wall is made up of H_2 selective Pd-alloy composite membrane. The membrane reactor configuration MR2 is H_2 selective membrane reactor with two packed reactor tubes each is identical to MR1. The reactor configurations MR3 and MR4 are the series combination of MR1 and PROX reactors, and MR2 and PROX reactors respectively.

For FBR1 and PROX reactors, the permeation flux J_i in Eq. (13) is set to zero. In case of MR1 and MR2, only one component H_2 gets permeated through membrane. Therefore, permeation flux (J_i) for all components except H_2 is set to zero in Eq. (13). For FBR1, MR1 and MR2, five gaseous components (CH_3OH, H_2O, H_2, CO, CO_2) are present in reaction zone. On permeation side of membrane reactors MR1 and MR2, there are only two components namely H_2 and steam as sweep gas. As a result, the mathematical model consists of five,

Table 4
Mathematical model equations for traditional fixed bed and membrane reactors.

(1) Reaction Zone (FBR1, MR1, MR2, PROX Reactor)

$$\frac{dF_{ti}}{dz} = \pi R_1^2 \rho_B \sum_{j=1}^{M} \eta_j (\pm \nu_{ij} r_j) - 2\pi R_1 J_i \qquad (13)$$

FBR1, MR1, MR2: $i = CH_3OH$, H_2O, H_2, CO, CO_2; $j = R_1$, R_2, R_3
$J_i = 0 \ i \neq H_2$
PROX Reactor: $i = O_2$, H_2, CO, CO_2, H_2O, N_2; $j = R_4$, R_5, R_6

(2) Permeation Zone (MR1, MR2)

$$\frac{dF_{si}}{dz} = 2\pi R_2 J_i \quad ; i = H_2 \qquad (14)$$

Boundary conditions ($z = 0$)

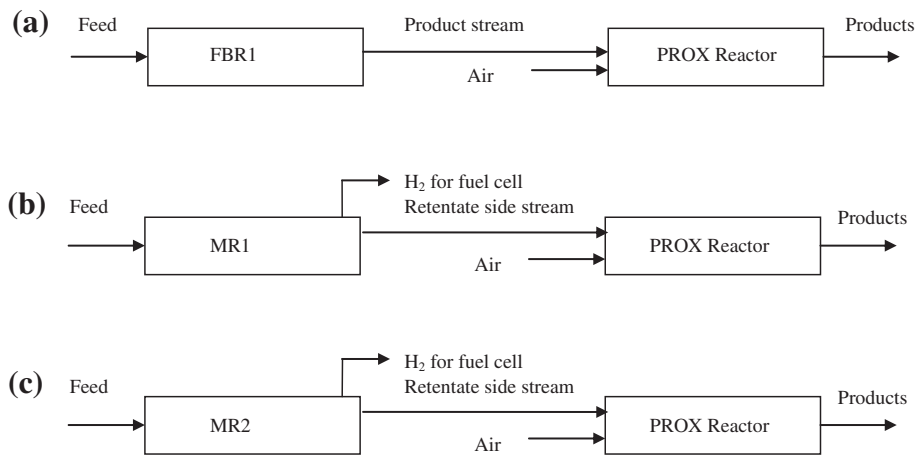| Reaction zone:	Permeation zone:
$F_{tCH_3OH,0} = 2 \times 10^{-3}$ mol s^{-1}	$F_{sH_2,0} = 0$
$F_{tH_2O,0} = S/M \times F_{0,CH_3OH}$	$F_{sS_g,0} = SR \times F_{CH_3OH,0}$
$F_{tH_2,0} = 10^{-9}$ mol s^{-1}	
$F_{tCO,0} = F_{CO_2,0} = 0$	

Fig. 2. Schematic representation of FBR2 (a), MR3 (b), and MR4 (c).

seven and seven ordinary differential equations (Eqs. (13) and (14)) for FBR1, MR1 and MR2 respectively. In the reformer, approximately complete conversion of methanol has been achieved at the given operating condition of temperature, S/M ratio and pressure. In view of this, the exit reformate gas from FBR1, MR1 and MR2 is considered to consist only four components H_2O, H_2, CO and CO_2. In the PROX reactor, air is co-fed with exit reformate gas for FBR2, MR3 and MR4 reactor configurations. Thus, the mathematical model for PROX reactor consists of six ordinary differential equations corresponding to six components. All the feed streams are introduced at the inlet end of the reactors FBR1, MR1, MR2 and PROX. In case of MR1 and MR2, steam as sweep gas is introduced into permeation zone (shell side) in co-current mode with respect to feed in reaction zone (tube side). Thus, all the boundary conditions required to solve the set of ordinary differential equations are available at the inlet end of all the reactors (Table 4). Therefore, model equations for all the reactor configurations constitute initial value problem. In the present study, the sets of ordinary differential equations for all the reactors are solved by using ode45 toolbox in MATLAB 7. During simulation of MR1 and MR2 reactors, the infinite rates of H_2 permeation at inlet conditions in Eq. (12) are avoided by adding negligible amount of H_2 (1×10^{-9} mol s^{-1}) in feed. The performance of all six reactor configurations is analyzed in terms of conversion of CH_3OH, yield of H_2 and recovery of H_2. The definitions of the parameters of interest in the present study are given below [34,51]

$$\text{Conversion of } CH_3OH(\%) = \left(\frac{F_{tCH_3OH,0} - F_{tCH_3OH,out}}{F_{tCH_3OH,0}} \right) \times 100 \quad (15)$$

$$\text{Yield of } H_2 = \left(\frac{F_{tH_2} + F_{sH_2}}{F_{tCH_3OH,0}} \right) \quad (16)$$

$$\text{Recovery of } H_2(\%) = \left(\frac{F_{sH_2}}{F_{sH_2} + F_{tH_2}} \right) \times 100 \quad (17)$$

5. Results and discussion

5.1. Model validation

The developed one dimensional comprehensive mathematical model for fixed bed reactor is validated with the results of experimental study by Peppley et al. [22] on methanol steam reforming.

Peppley et al. [22] conducted the experiments on methanol steam reforming in a fixed bed reactor with $CuO/ZnO/Al_2O_3$ catalyst at temperature ranging between 433 and 533 K, S/M ratio of 1 in feed, and total pressure of 1 bar. The conversion of methanol at various $W/F_{tCH_3OH,0}$ values was measured by ensuring that the catalyst activity had remained stable during the experiment. As stated in the previous section, Peppley et al. [22] considered three reactions namely methanol steam reforming, methanol decomposition and WGS reaction. In the present study, the model equations (Eq. (13)) written for each reaction component, are solved for the same operating conditions and kinetic expressions as used by Peppley et al. [22]. The comparison of model predictions and experimental results is shown in Fig. 3. It can be seen that the model predictions are in good agreement with the experimental results. Thus, the developed mathematical model for methanol steam reforming to produce H_2, simulates the laboratory reactor very well.
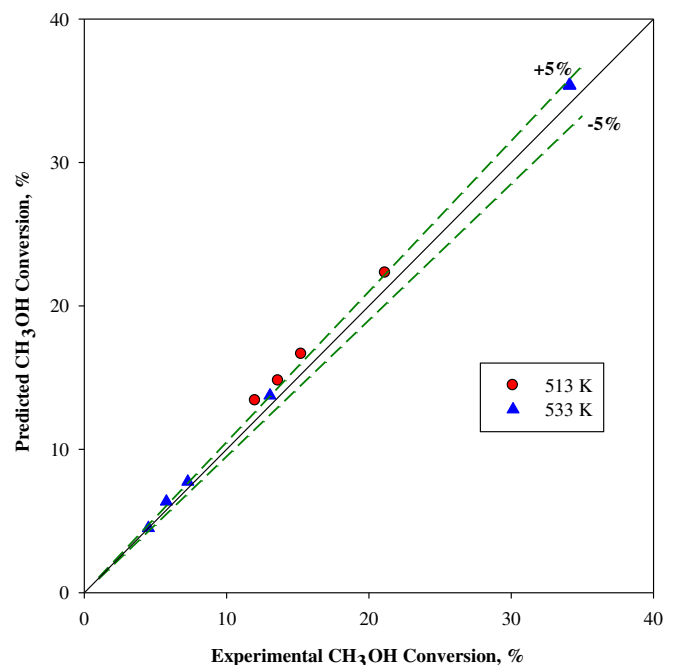

Fig. 3. Experimental and predicted methanol conversion results for model validation.

5.2. Simulation of FBR1, MR1 and MR2 reactor configurations

The methanol steam reforming on Cu-based catalyst is carried out at lower temperature due to limitations of the Cu-based catalysts. According to the thermodynamic study on methanol steam reforming carried out by Katiyar et al. [8], the maximum H_2 yield with complete conversion of methanol can be achieved at S/M molar ratio of 1.5 in feed, temperature of 450 K and pressure of 1 bar. In view of these facts and findings, the present simulation study is carried out at S/M ratio of 1.5, pressure of 1 bar and reforming temperature between 473 and 600 K. These conditions are considered as sufficient to achieve complete conversion of methanol in the reformer. In the simulation of all six reactor configurations, the reformer is assumed to be operated near isothermal condition by supplying heat externally through wall. All operating conditions required for simulation are mentioned in Table 3. The performance of six reactor configurations is compared in terms of H_2 yield, CO concentration and CO free H_2 production (H_2 recovery) for PEM fuel cell application.

The effect of temperature on methanol conversion in FBR1 at S/M ratio of 1.5 and pressure of 1 bar is shown in Fig. 4. The methanol conversion is favored by higher reforming temperature due to overall endothermicity of the reactions. 99.52% conversion is achieved at 593 K. High pressure does not favor the SRM and MD reactions as the moles are increasing with the progress of reaction. Therefore, the methanol conversion of 97.88% is achieved at pressure of 2 bar which is less than at 1 bar (99.52%).

The variation in molar flow rate of reaction components with contact time values (0.5–10 kg_{cat} s mol^{-1}) considered in FBR1 at temperature of 593 K is shown in Fig. 5(a). H_2 yield of 2.67 is obtained which is less than theoretical yield of 3 (Table 5). It is known that at temperature less than 600 K, the contribution of MD to produce H_2 is smaller than SRM. This results in lower value of CO than of CO_2, and H_2 yield not close to 3 even at approximately complete conversion of methanol in FBR1. However, the concentration of CO in ppm is very high and requires further reduction before feeding to PEM fuel cell. In order to modify H_2 yield and CO concentration, the membrane reactor configuration (MR1) is considered. In the packed bed reactor, the central packed reaction tube is made up of H_2 selective Pd/Ag alloy membrane through which a part of produced H_2 gets permeated from reaction side to permeation side. The performance of the membrane reactor is measured in terms of H_2 recovery from permeate side and CO concentration in the retentate side of the reactor.

The removal of H_2 through membrane shifts the equilibrium of all three reactions (R_1-R_3) toward product formation. The final
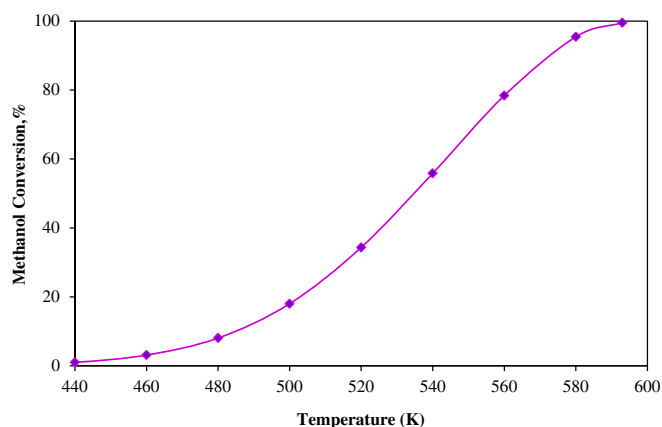
concentrations of the products and percent H_2 recovery from permeation side depend upon the H_2 permeation rate through membrane. The driving force for permeation which is trans-membrane pressure difference can be increased by lowering the partial pressure of H_2 at permeation side. The sweep gas flow through permeation zone helps in reducing the partial pressure of H_2 there. Higher is the sweep gas flow rate, lower will be H_2 partial pressure. The sweep gas flow rate is decided on the basis of sweep ratio defined as the molar ratio of sweep gas flow rate to methanol flow rate in feed. In the present study, widely used sweep ratio range (1–10) is considered with steam as sweep gas. The advantage is that the steam can be easily separated from the permeated H_2 by the condensation process. The simulated H_2 recovery obtained at different sweep ratios is shown in Fig. 6 for MR1. It is clear that sweep ratio favors H_2 recovery. At sweep ratio higher than 4, however, the increase in H_2 recovery is not significant. In the literature also, it was reported that at sweep ratio greater than 5:1, the H_2 recovery was found to be almost constant and therefore no relevant benefits were achieved [34,52,53]. In view of these findings, the sweep ratio of 4 is set for simulations of all membrane reactor configurations in the present study.

The simulation of membrane reactor configuration MR1 is carried out at pressure of 2 bar in reaction side and of 1 bar in permeation side keeping other operating parameters same as mentioned in Table 3. The selective removal of H_2 from reaction side through membrane not only shifts the reaction equilibrium toward product formation resulting in more conversion of reactant, but also it reduces the endothermic reforming temperature to achieve the same conversion. Similar fact has also been demonstrated thermodynamically by Katiyar et al. [8]. In MR1, 99.20% conversion is achieved at temperature of 593 K whereas in FBR1 at 2 bar pressure, the methanol conversion of 97.88% is achieved at 593 K. The variation in molar flow rates of all the components with residence time (kg_{cat} s mol^{-1}) for MR1 is illustrated in Fig. 5(b). The molar flow rate of H_2 in reaction side first increases due to high production rate of H_2 and then decreases due to high permeation rate of H_2 through membrane. On the other hand, the concentration of H_2 in permeation side continuously increases. Since the permeation of H_2 favors the WGS reaction, the concentration of CO gets reduced while the yield of H_2 and molar flow rate of CO_2 get increased (from 1.37×10^{-3} to 1.48×10^{-3} mol s^{-1}) in comparison to FBR1. The recovery of H_2 is found to be 50.43 mol% with H_2 yield of 2.72 as shown in Table 5.

Beside the permeation driving force, an alternative way to further improve H_2 recovery and to reduce CO concentration, is the enhancement in the residence time in the reaction zone. High residence time affects in two ways. First, it increases the conversion of methanol (R_1 and R_2) and CO (R_3) to produce more H_2 resulting in more permeation of H_2 through membrane. Secondly, it provides sufficient time for H_2 permeation through membrane. It is known that the residence time of reaction mixture in reaction zone is related to the total feed flow rate. Low feed flow rate leads to increase in residence time in the reactor. This fact is implemented in next membrane reactor configuration MR2 by employing two identical reaction tubes in parallel (Fig. 1(c)). Thus, half of the total feed is introduced in each reaction tube. The reactor configuration MR2 is simulated at identical operating conditions as MR1 (Table 3). The molar flow rate profiles are shown in Fig. 5(c). Table 5 gives the values of other simulated parameters for MR2. It is clear from Fig. 5(c), that a large part of produced H_2 gets permeated through membrane. As a result, small amount of H_2 is left in reaction side in comparison to MR1. More CO_2 production is caused by large CO consumption via WGS reaction in MR2. From Table 5, it can be seen that 91.25 mol% of produced H_2 is recovered from permeation side as CO free H_2. Due to high H_2 removal, high methanol conversion

Fig. 4. Effect of temperature on methanol conversion at 1 bar pressure and S/M molar ratio of 1.5.
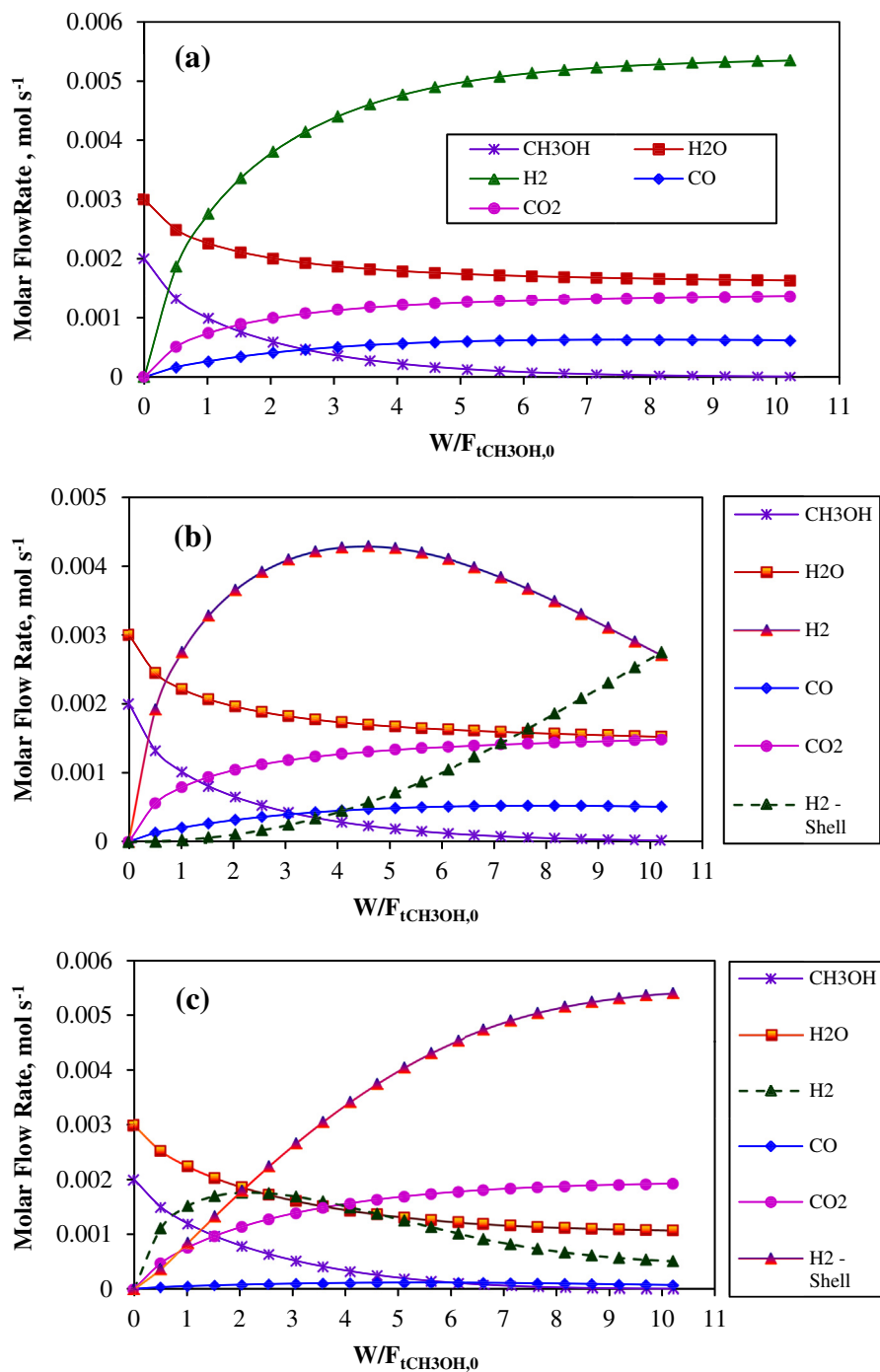
Fig. 5. Component molar flow rates as a function of $W/F_{tCH_3OH,0}$ ratio at $S/M = 1.5$ for (a) FBR1: $T = 593$ K and $P_t = 1$ bar, (b) MR1: $T = 593$ K, $P_t = 2$ bar and $P_s = 1$ bar, (c) MR2: $T = 560$ K, $P_t = 2$ bar and $P_s = 1$ bar.

(99.81%) is achieved at lower temperature of 560 K and more CO is converted to H_2 via WGS reaction, yielding lower CO concentration as 8016 ppm compared to MR1. In MR2, the H_2 yield of 2.96 is achieved which is very close to the theoretical yield of 3. Thus, it

may be concluded that high residence time has a notable influence on the H_2 yield, H_2 recovery and concentration of CO.

5.3. Simulation of FBR2, MR3 and MR4 reactor configurations

The above results show that 50.43 mol% H_2 recovery from the permeate side of MR1 provides small amount of CO free hydrogen for PEM fuel cell application. Also, the exit concentration of CO from FBR1 and retentate side of MR1 is very high for feeding to fuel cell. In order to make the exit product stream suitable for PEM fuel cell application, PROX reactor is attached to FBR1 and MR1 to form reactor configurations FBR2 and MR3 respectively. In case of MR2,

Table 5
Simulation results of reactor configurations.

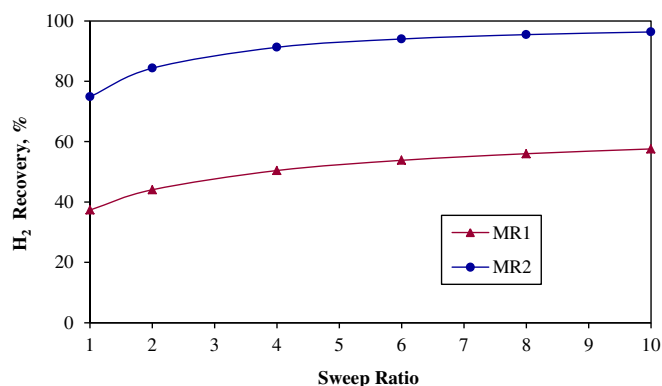| Reactor configuration	T (K)	P (bar)	CH$_3$OH conversion, %	Yield of H$_2$	CO (ppm)	H$_2$ recovery, %
FBR1	593	$P_t = 1$	99.52	2.67	69,350	–
MR1	593	$P_t = 2, P_s = 1$	99.20	2.72	56,310	50.43
MR2	560	$P_t = 2, P_s = 1$	99.81	2.96	8016	91.25

Fig. 6. Effect of sweep ratio on H_2 recovery in MR1 and MR2.

91.25 mol% H_2 recovery from the permeation side provides sufficient CO free hydrogen for the purpose of feeding to PEM fuel cell. The retentate stream from MR2 contains CO, CO_2, H_2 and H_2O. If this stream is obtained from an industrial reformer, it can be utilized after further processing for the production of useful products. But, for portable PEM fuel cell application, this option is not viable. At the same time, it is not advisable to release these gases into the environment with the present composition as it contains CO more than 9 ppm [54]. Therefore, it is necessary to convert CO into safe and harmless products before releasing to the environment. For this purpose, a PROX reactor is attached to MR2 in reactor configuration MR4. The simulation results of FBR2, MR3 and MR4 are discussed in the following paragraphs.

In FBR2, MR3 and MR4 reactor configurations, the exit streams from FBR1, MR1 and MR2 respectively are fed to PROX reactor. The PROX reactor is simulated at O_2/CO ratio ranging between 1 and 2. The rate of air feed for O_2 is decided by CO flow rate and O_2/CO ratio. The PROX reactor is simulated at 1 bar pressure for FBR2 and at 2 bar pressure for MR3 and MR4 reactor configurations. The PROX reactor dimensions are same as given in Table 3. The results of PROX reactors are compiled in Table 6. The temperature mentioned in Table 6 refers to CO conversion greater than 99.9% at different O_2/CO ratios. Since exit flow rate of CO is different in FBR1 (6.24×10^{-4} mol s^{-1}), MR1 (5.05×10^{-4} mol s^{-1}), and MR2 (7.21×10^{-5} mol s^{-1}), the flow rate of O_2 varies in each reactor configuration at one value of O_2/CO ratio. The oxidation of CO and consequent oxidation of H_2 increase at higher O_2/CO ratio resulting in reduction in CO concentration and consequently in temperature. This type of trend is found in all three reactor configurations FBR2, MR3 and MR4. However in MR4, the temperature is far less than the temperature attained in FBR2 and MR3. In FBR2, the H_2 flow rate is higher in the exit stream from FBR1 whereas due to recovery of H_2, the flow rate of H_2 in the exit streams from MR1 and MR2 is less. The low temperature and low concentrations of CO and H_2 in MR3

and MR4 reduce the possibility of methanation and RWGS reactions. It is clear from Table 6 that in FBR2 and MR3 reactor configurations, the maximum CO concentration is reduced to 41.7 ppm and 24.6 ppm respectively at O_2/CO ratio of 2. On the other hand in MR4, CO concentration of 4.1 ppm is achieved at O_2/CO ratio of 2 and temperature of 423 K which meets out the permissible composition requirement for safe release to the environment. Although consumption of H_2 in PROX reactor is shown higher for MR4, net H_2 consumption and formation of H_2O are very much less in comparison to FBR2 as 91.25 mol% recovery of H_2 has been achieved from permeation side of MR2.
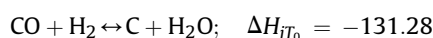
5.4. Qualitative analysis of carbon formation

The formation of carbon during the catalytic methanol reforming reaction leads to deactivation of catalyst, resulting in low catalyst durability and activity. The most probable and thermodynamically favorable carbon formation reactions at given operating conditions are listed below:
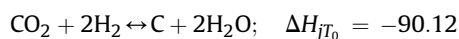
Boudouard Reaction (R_7)

$$2CO \leftrightarrow CO_2 + C; \quad \Delta H_{jT_0} = -172.45$$

CO reduction reaction (R_8)

$$CO + H_2 \leftrightarrow C + H_2O; \quad \Delta H_{jT_0} = -131.28$$

CO_2 reduction reaction (R_9)

$$CO_2 + 2H_2 \leftrightarrow C + 2H_2O; \quad \Delta H_{jT_0} = -90.12$$

The thermodynamic criteria help to identify the tendency of carbon formation on the catalyst surface by reactions. In the present study, the thermodynamic criteria based on carbon activity to predict the carbon formation are employed. The carbon activity is defined on the basis of principle of equilibrated gas. It is noted that the carbon activity is only the indicator for the presence of carbon in the stream, and it does not give the information regarding the amount of carbon formation [55]. All three carbon formation reactions (R_7–R_9) are employed to examine the thermodynamic possibility of carbon formation by estimating the values of carbon activity in three reactions. The carbon activity (ϕ_j) of each reaction is defined as follows:

$$\phi_{R_7} = \frac{K_{R_7,T}}{\psi_1}; \quad \psi_1 = \frac{p_{tCO_2}}{p_{tCO}^2} \tag{18}$$

$$\phi_{R_8} = \frac{K_{R_8,T}}{\psi_2}; \quad \psi_2 = \frac{p_{tH_2O}}{p_{tCO}p_{tH_2}} \tag{19}$$

$$\phi_{R_9} = \frac{K_{R_9,T}}{\psi_3}; \quad \psi_3 = \frac{p_{tH_2O}^2}{p_{tCO_2}\,p_{tH_2}^2} \tag{20}$$

In Eqs. (18)–(20), $K_{R_7,T}, K_{R_8,T}$, and $K_{R_9,T}$ represent equilibrium constants for reactions R_7–R_9 respectively and are taken from the studies of Katiyar et al. [8]. The ψ_1–ψ_3 are the parameters defined in terms of partial pressures of reactants and products in the respective reactions. Since all the three reactions are reversible, the carbon formation and the gasification of carbon occur simultaneously. The carbon activity greater than unity ($\phi_j > 1$) indicates that the reaction has not yet reached the thermodynamic

Table 6
Simulation results of PROX reactor in reactor configurations FBR2, MR3 and MR4.

Reactor configuration	O_2/CO	T (K)	P (bar)	CO (ppm)	% H_2 consumption
FBR2	1	583	1	54.5	7.6
	1.5	559	1	47.2	8.7
	2	548	1	41.7	9.4
MR3	1	516	2	48.5	9.9
	1.5	506	2	33.6	13.7
	2	501	2	24.6	16.3
MR4	1	450	2	9.5	13.7
	1.5	431	2	7.3	19.2
	2	423	2	4.1	22.4

Table 7
Carbon formation simulation results.

Reactor configurations	T (K)/P (bar)	Carbon activity ϕ_j for reactions		
		ϕ_{R_7}	ϕ_{R_8}	ϕ_{R_9}
FBR1	593/1	2.89×10^4	0.65×10^4	0.15×10^4
MR1	593/2	5.06×10^4	0.82×10^4	0.14×10^4
MR2	560/2	1.09×10^4	0.27×10^4	0.07×10^4

equilibrium. Alternatively, ϕ_j less than unity indicates that the carbon formation will not be thermodynamically favored by jth reaction.

The risk of carbon deposition on methanol steam reforming catalyst is evaluated in FBR1, MR1 and MR2 reactor configurations by each carbon formation reactions on the basis of ϕ_j values at given operating conditions. The simulated results are mentioned in Table 7. For the selected operated conditions, the minimum tendency of carbon formation is found by R_9 and maximum by R_7 in all reactor configurations. The behavior of results mentioned in Table 7 can be explained on the basis of stoichiometry of reactions R_7–R_9, and temperature and pressure conditions. The reduction in partial pressure caused by H_2 permeation through membrane decreases the risk of carbon formation by reactions R_8 and R_9. Conversely, the high pressure and low temperature in membrane reactor favor the carbon formation by reactions R_7–R_9. In case of MR1, low removal of H_2, high CO concentration (Table 5), and high pressure lead to enhance the risk of carbon formation by R_7 in comparison to FBR1. In MR2 reactor configuration, very high removal of H_2 through membrane reduces the rates of reactions R_8 and R_9 to a great extent and also promotes WGS reaction which results in reduction in CO content as given in Table 5. The high reduction in CO suppresses the carbon formation by reactions R_7 and R_8. In view of these findings, it can be concluded that the risk of carbon deposition on reforming catalyst is minimum in the case of MR2 reactor configuration.

5.5. Suitability for PEM fuel cell

In the above simulation results, the steam is used as sweep gas in membrane reactor which can be removed from H_2 by condensation. It is known that PEM fuel cell fueled by humidified H_2 performs better than that fueled by stored dry H_2. Therefore, if after condensation, some water is remained in H_2 it will be beneficial to PEM fuel cell operation. Secondly, the fuel cell start up performance is improved by humidified H_2 in comparison to stored dry H_2 as reported by Wang et al. [56]. The aforementioned results demonstrate that pure H_2 yield of 2.7 is obtained from the permeate side of the MR4 reactor configuration at temperature of 560 K, which can be directly fed to PEM fuel cell anode. This amount is equivalent to 7.4 NL min^{-1} of H_2 generation from 0.12 mol min^{-1} of methanol in feed with S/M ratio of 1.5. According to literature [17,57], this H_2 generation can fulfill 470 W PEM fuel cell H_2 feedstock requirement.

6. Conclusions

A comprehensive simulation analysis of fuel processor based on methanol steam reforming for fuel cell grade H_2 production has been presented. Six reactor configurations namely FBR1 (fixed bed reactor), MR1 (membrane reactor with one reaction tube), MR2 (H_2 selective membrane reactor with two reaction tubes), FBR2 (FBR1 + PROX), MR3 (MR1 + PROX), and MR4 (MR2 + PROX) are compared to assess the suitable process scheme. The simulation is carried out at steam to methanol ratio of 1.5, pressure 1–2 bar. In the fixed bed reactor (FBR1), complete conversion of methanol is

achieved at 593 K with H_2 yield of 2.67 and CO concentration of 69,350 ppm. In FBR2, FBR1 is connected with PROX reactor. CO concentration and consequently H_2 yield are reduced to 41.7 ppm and 2.42 respectively at O_2/CO ratio of 2. This composition is not suitable for PEM fuel cell stack. The performance is improved by carrying out the methanol steam reforming in H_2 selective membrane reactor at 2 bar pressure keeping 1 bar pressure in the permeate side. Steam is used as a sweep gas in membrane reactor since PEM fuel cell fueled by humidified H_2 performs better. It is demonstrated that in MR1 complete conversion of methanol, H_2 yield (2.72), and CO concentration (56,310 ppm) at temperature of 593 K are positively affected by the presence of membrane. 50.43 mol% recovery of H_2 is achieved from the permeate side of MR1 which is low to feed directly to fuel cell stack. CO concentration is further reduced by attaching PROX reactor with MR1 in MR3 reactor configuration. CO concentration is further reduced from 56,310 to 24.6 ppm at O_2/CO ratio of 2 in PROX reactor which is much higher for feeding to fuel cell. In MR2 reactor configuration, two identical reaction tubes are used in order to increase the residence time of reacting stream. It is demonstrated that enhancement in residence time effects the performance of reactor significantly. The H_2 yield of 2.96 which is close to theoretical yield of 3 and 91.25 mol% recovery of H_2 from the permeate side of MR2 are achieved at temperature of 560 K. The retentate gases contains very small amount of H_2 and CO of 8016 ppm. The CO concentration is reduced to 4.1 ppm at O_2/CO ratio of 2 in a PROX reactor of MR4 reactor configuration for safe release to the environment. Carbon formation analysis reveals that carbon formation tendency is quite low in H_2 selective membrane reactor with two identical reaction tubes in comparison to other reactor configurations. From MR4 reactor configuration 7.4 NL min^{-1} of pure H_2 can be fed directly to PEM fuel cell which fulfills 470 W fuel cell stack requirement.

Nomenclature

D_1	inner diameter of tube (m)
Dp	catalyst particle diameter (m)
$F_{ti,0}$	molar flow rate of ith component in feed in tube side (mol s^{-1})
F_{ti}	molar flow rate of ith component in tube side (mol s^{-1})
$F_{si,0}$	molar flow rate of ith component in feed in shell side (mol s^{-1})
F_{si}	molar flow rate of ith component in shell side (mol s^{-1})
ΔH_{jT_0}	enthalpy of jth reaction at standard temperature ($T_0 = 298$ K), (kJ mol^{-1})
J_{H_2}	hydrogen flux (mol m^{-2} s^{-1})
K_{jT}	equilibrium constant for jth reaction at temperature T
L	reactor length (m)
P_t	tube side total pressure (bar)
P_s	shell side total pressure (bar)
p_{ti}	tube side partial pressure of component i (bar)
p_{si}	shell side partial pressure of component i (bar)
P_{MH_2}	hydrogen permeation coefficient (mol m^{-1} s^{-1} bar$^{-0.5}$)
$P_{MH_2,0}$	pre-exponential factor in Eq. (10) (mol m^{-1} s^{-1} bar$^{-0.5}$)
r_j	rate of jth reaction (mol kg$_{cat}^{-1}$ s^{-1})
r_i	net rate of formation of ith component in the reformer (mol kg$_{cat}^{-1}$ s^{-1})
r_i^*	net rate of formation of ith component in PROX reactor (mol kg$_{cat}^{-1}$ s^{-1})
R	gas constant (J mol^{-1} K^{-1})
T	temperature (K)

Greek Letters

ρ_B	bulk density of reforming catalyst (kg m^{-3})
δ	membrane thickness (m)

ν_{ij}	stoichiometric coefficient of *i*th component in *j*th reaction
β_C	correction factor in Eq. (11)
η_j	effectiveness factor of *j*th reaction
ϕ_j	carbon activity for *j*th reaction

Abbreviations

MD	Methanol decomposition
PROX	Preferential oxidation of CO
SRM	Steam reforming of methanol
S/M	Steam to methanol molar ratio in feed
SR	Sweep ratio (sweep gas/methanol molar ratio)
WGS	Water gas shift

References

[1] M.L. Rodríguez, M.N. Pedernera, D.O. Borio, Catal. Today 193 (2012) 137−144.
[2] Y. Choi, H.G. Stenger, J. Power Sourc. 142 (2005) 81−91.
[3] J. Agrell, H. Birgersson, M. Boutonnet, J. Power Sourc. 106 (2002) 249−257.
[4] M.F. Demirbas, M. Balat, H. Balat, Energ. Convers. Manage. 52 (4) (2011) 1815−1828.
[5] S. Patel, K.K. Pant, Fuel Process. Technol. 88 (2007) 825−832.
[6] S.D. Jones, L.M. Neal, H.E. Hagelin-Weaver, Appl. Catal. B 84 (2008) 631−642.
[7] S. Ahmed, M. Krumpelt, Int. J. Hydrogen Energy 26 (2001) 291−301.
[8] N. Katiyar, S. Kumar, S. Kumar, Int. J. Hydrogen Energy 38 (2013) 1363−1375.
[9] G. Avgouropoulos, J. Papavasiliou, T. Ioannides, Chem. Eng. J. 154 (2009) 274−280.
[10] C. Qi, J.C. Amphlett, B.A. Peppley, J. Power Sourc. 171 (2007) 842−849.
[11] T. Valdés-Solís, G. Marbán, A.B. Fuertes, Catal. Today 116 (2006) 354−360.
[12] T. Shishido, Y. Yamamoto, H. Morioka, K. Takehira, J. Mol. Catal. A Chem. 268 (2007) 185−194.
[13] H. Jeong, K.I. Kim, T.H. Kim, C.H. Ko, H.C. Park, I.K. Song, J. Power Sourc. 159 (2006) 1296−1299.
[14] S. Sá, J.M. Sousa, A. Mendes, Chem. Eng. Sci. 66 (2011) 5523−5530.
[15] M.P. Harold, B. Nair, G. Kolios, Chem. Eng. Sci. 58 (2003) 2551−2571.
[16] J.R. Hufton, S. Mayorga, S. Sircar, AIChE J. 45 (1999) 248−256.
[17] M.D. Falco, Fuel 90 (2011) 739−747.
[18] S. Sá, J.M. Sousa, A. Mendes, Catal. Today 156 (2010) 254−260.
[19] D. Lee, S. Park, C. Yu, S. Ihm, K. Lee, J. Memb. Sci. 316 (2008) 63−72.
[20] S.H. Israni, M.P. Harold, J. Memb. Sci. 369 (2011) 375−387.
[21] G.Q. Lu, J.C.D.D. Costa, M. Duke, S. Giessler, R. Socolow, R.H. Williams, T. Kreutz, J. Colloid Interface Sci. 314 (2007) 589−603.
[22] B.A. Peppley, J.C. Amphlett, L.M. Kearns, R.F. Mann, Appl. Catal. A 179 (1999) 31−49.
[23] V. Agarwal, S. Patel, K.K. Pant, Appl. Catal. A 279 (2005) 155−164.
[24] R. Chein, L. Chen, Y. Chen, J.N. Chung, Int. J. Hydrogen Energy 34 (2009) 5398−5408.
[25] Y. Li, W. Lin, L. Yu, Z. Hao, R. Mai, J. Nat. Gas Chem. 17 (2008) 171−174.
[26] A. Mastalir, B. Frank, A. Szizybalski, H. Soerijanto, A. Deshpande, M. Niederberger, J. Catal. 230 (2005) 464−475.
[27] S. Patel, K.K. Pant, Chem. Eng. Sci. 62 (2007) 5425−5435.
[28] H. Purnama, T. Ressler, R.E. Jentoft, H. Soerijanto, R. Schlögl, R. Schomäcker, Appl. Catal. A 259 (2004) 83−94.
[29] S.H. Israni, M.P. Harold, Ind. Eng. Chem. Res. 49 (2010) 10242−10250.
[30] F. Gallucci, S. Tosti, A. Basile, J. Memb. Sci. 317 (2008) 96−105.
[31] M.C.J. Bradford, M.A. Vannice, Appl. Catal. A 142 (1996) 97−122.
[32] J.P. Collins, J.D. Way, Ind. Eng. Chem. Res. 32 (1993) 3006−3013.
[33] F. Gallucci, M.D. Falco, S. Tosti, L. Marrelli, A. Basile, Int. J. Hydrogen Energy 32 (2007) 4052−4058.
[34] F. Gallucci, A. Basile, Int. J. Hydrogen Energy 33 (2008) 1671−1687.
[35] A. Unemoto, A. Kaimai, K. Sato, T. Otake, K. Yashiro, J. Mizusaki, T. Kawada, T. Tsuneki, Y. Shirasaki, I. Yasuda, Int. J. Hydrogen Energy 32 (2007) 2881−2887.
[36] A. Unemoto, A. Kaimai, K. Sato, T. Otake, K. Yashiro, J. Mizusaki, T. Kawada, T. Tsuneki, Y. Shirasaki, I. Yasuda, Int. J. Hydrogen Energy 32 (2007) 4023−4029.
[37] F. Gallucci, F. Chiaravalloti, S. Tosti, E. Drioli, A. Basile, Int. J. Hydrogen Energy 32 (2007) 1837−1845.
[38] T.A. Peters, M. Stange, H. Klette, R. Bredesen, J. Memb. Sci. 316 (2008) 119−127.
[39] A.L. Mejdell, M. Jøndahl, T.A. Peters, R. Bredesen, H.J. Venvik, Sep. Purif. Technol. 68 (2009) 178−184.
[40] G. Barbieri, F. Scura, F. Lentini, G.D. Luca, E. Drioli, Sep. Purif. Technol. 61 (2008) 217−224.
[41] B.A. Wilhite, M.A. Schmidt, K.F. Jensen, Ind. Eng. Chem. Res. 43 (2004) 7083−7091.
[42] F. Gallucci, L. Paturzo, A. Basile, Ind. Eng. Chem. Res. 43 (2004) 2420−2432.
[43] J.R. Lattner, M.P. Harold, Catal. Today 120 (2007) 78−89.
[44] E. Gobina, K. Hou, R. Hughes, J. Memb. Sci. 105 (1995) 163−176.
[45] J.J. Carberry, M.M. Wendel, AIChE J. 9 (1963) 129−133.
[46] J.S. Oklany, K. Hou, R. Hughes, Appl. Catal. A 170 (1998) 13−22.
[47] G.F. Froment, K.B. Bischoff, Chemical Reactor Analysis and Design, second ed., Wiley, New York, 1990.
[48] G. Barbieri, F.P.D. Maio, Ind. Eng. Chem. Res. 36 (1997) 2121−2127.
[49] J. Shu, B.P.A. Grandjean, S. Kaliaguine, Appl. Catal. A 119 (1994) 305−325.
[50] K. Hou, M. Fowles, R. Hughes, Chem. Eng. Sci. 54 (1999) 3783−3791.
[51] H.S. Fogler, Elements of Chemical Reaction Engineering, third ed., Prentice Hall, New Jersey, 1999.
[52] A. Iulianelli, T. Longo, A. Basile, Int. J. Hydrogen Energy 33 (2008) 5583−5588.
[53] S. Sá, H. Silva, J.M. Sousa, A. Mendes, J. Memb. Sci. 339 (2009) 160−170.
[54] http://inspectapedia.com/hazmat/Carbon_Monoxide_Exposure_Limits.htm.
[55] S. Assabumrungrat, N. Laosiripojana, P. Piroonlerkgul, J. Power Sourc. 159 (2006) 1274−1282.
[56] E. Wang, P. Shi, C. Du, X. Wang, J. Power Sourc. 181 (2008) 144−148.
[57] Y. Kim, Y. Kim, S. Yeo, K. Kim, K.J. Koh, J. Seo, S.J. Shin, D. Choi, C.W. Yoon, S.W. Nam, J. Power Sourc. 229 (2013) 170−178.